Regular Article

PHYSICAL CHEMISTRY RESEARCH
Published by the
Iranian Chemical Society
www.physchemres.org
info@physchemres.org

Phys. Chem. Res., Vol. 12, No. 3, 675-691, September 2024
DOI: 10.22036/pcr.2023.426148.2451

Exploring the Interactions of Natural Flavonoids with COX-2: Insights from Molecular Docking, DFT Analysis, and ADME Calculations

N. Lachi[a], M. Cheriet[b,*] and N. Djadi[c,d]

[a]*Laboratory of Computational Chemistry and Nanostructures, Department of Material Sciences, Faculty of Mathematical, Informatics and Material Sciences, University of 8 May 1945, Guelma, Algeria*

[b]*Biotechnology Research Center-C.R.Bt, Constantine, Algeria*

[c]*Materials Chemistry Laboratory of Constantine, Department of Chemistry, Faculty of Pure Sciences, University of frères Mentouri Constantine 1*

[d]*Department of Chemistry, Faculty of Matter Sciences, University of Batna 1, Algeria*

(Received 20 November 2023, Accepted 10 December 2023)

This comprehensive study delves into the inhibitory properties of various natural flavonoids against cyclooxygenase-2 (COX-2), a crucial enzyme in the inflammatory pathway. Non-steroidal anti-inflammatory drugs (NSAIDs) are commonly employed to alleviate pain by targeting the COX enzyme. Employing molecular docking techniques, with established drugs like celecoxib, rofecoxib, and valdecoxib as benchmarks, the investigation assessed the interaction patterns of natural flavonoids. Notably, flavanone demonstrated a robust interaction with key residues TYR 385 and SER 530. Additionally, Density Functional Theory (DFT) and ADME calculations were employed to analyze structures with optimal affinities. These insights significantly contribute to discerning the potential therapeutic applications of natural compounds in COX-2 inhibition, offering promising avenues for future research and drug development.

Keywords: Flavonoids, COX-2, Molecular Docking, ADME studies, DFT

INTRODUCTION

Various physiological and pathological processes, including inflammation, atherosclerosis, tissue damage, angiogenesis, and tumorigenesis, are significantly influenced by the presence of the inducible enzyme Cyclooxygenase-2 (COX-2) [1,2]. Selective COX-2 inhibitors have been shown to be effective in preventing inflammation, proliferation, and angiogenesis, while simultaneously inducing apoptosis in human cells. In addition, studies show that COX-2 inhibitors have additive or synergistic effects when used in combination with current chemotherapeutic and targeted agents [3,6].

At the molecular level, the COX-2 active site contains critical amino acids such as arginine 120 and tyrosine 355, which are essential for the conversion of arachidonic acid into prostaglandins linked to inflammation. Understanding how standard drugs interact with COX-2 at this precise site is crucial. These drugs bind to the active site, disrupting COX-2 function and interrupting prostaglandin synthesis. This disruption forms the basis of the anti-inflammatory and analgesic effects of these drugs, underlining the importance of research into the COX-2 active site and its drug interactions for the development of therapies targeting inflammation and pain management [7-11].

In this context, natural flavonoids have acquired significant importance in scientific research due to their numerous effects. Various flavonoids have different properties, including anti-cancer, anti-inflammatory, anti-microbial, antioxidant, and even anti-viral [12-14]. These compounds have a basic benzo-pyrone structure (C6-C3-C6),

*Corresponding author. E-mail: mouna.cheriet@gmail.com

with the A and B rings linked by a three-carbon C ring (Fig. 1). Recognising the potential of flavonoids to inhibit key cellular signaling pathways, including COX-2, increasing interest is emerging in their therapeutic applications, either as stand-alone agents or in conjunction with existing chemotherapeutic agents [15,16]. Therefore, our main research objective was to evaluate the efficacy of natural flavonoid compounds known for their anti-inflammatory properties. We sought to understand their binding motifs with COX-2 enzymes using molecular docking simulations [17-19].

Our analysis included the identification of the flavonoid with the highest binding affinity to COX-2, as presented in Table S1 of the supplementary data. The main objective of this study is to elucidate the profile of these natural flavonoids as COX-2 inhibitors with the aim of attenuating inflammation responses [20].

To achieve this objective, we sought to elucidate the binding modes and affinities of different flavonoids with COX-2 using molecular docking simulations. In addition, we carried out a comparative analysis of the binding interactions between natural flavonoids and selective COX-2 inhibitors, such as Celecoxib, Rofecoxib, and Valdecoxib [21,22].

In addition, we integrated Density Functional Theory (DFT), a prevalent quantum chemical approach, into our analysis. After completing the docking process, we used the DFT method B3LYP/6-31G(d,p) as a post-selection tool to calculate Frontal Molecular Orbitals (FMOs) and Molecular Electrostatic Potentials (MEPs) for the selected structures [23-32]. This in-depth analysis provided valuable information on the electronic and electrostatic properties of these selected structures, improving our understanding of their chemical characteristics and reactivity.

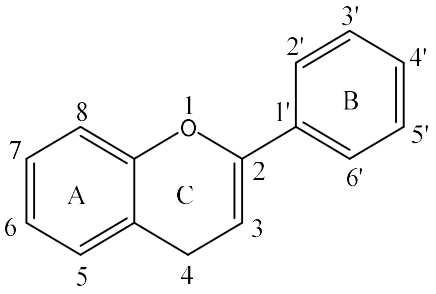

Fig. 1. Illustrates the fundamental chemical structure of flavonoids.

MATERIALS AND METHODS

Molecular docking experiments employed Autodock Vina 1.1.2 [33], a widely used semi-flexible docking algorithm that takes into account the ligand flexibility by adjusting its conformation within the active site while keeping the protein rigid. For the docking studies conducted in this research, thirty-five natural flavonoids and three synthetic COX-2 blockers, specifically Coxibs (Celecoxib, Rofecoxib, and Valdicoxib), were chosen as test compounds. The PubChem database was used to retrieve the 3D structures of all these compounds in sdf format, which were later converted to PDB format using the Discovery Studio 2021 software [34]. The Gasteiger charges were then added using Auto Dock Tools1.5.7 [35], and the energy of the compound structures was minimized. To prepare the proteins, crystal structures of selected COX-2 proteins were extracted from the RCSB Protein Database, and a grid, centered on the co-crystallized ligand with a span of 40 Å and a grid spacing of 0.375 Å, was generated to cover the entire protein-binding site (Table 1). The interaction mode prediction was evaluated using the Root Mean Square Deviation (RMSD) of the designed model generated by the software relative to the structure of the reference ligand. The docking experiments were performed using Auto Dock Vina with default settings, and the resulting structures from docking were analyzed using Discovery Studio Visualizer, which allowed visualization of the ligand-receptor interactions in 3D space. Density Functional Theory (DFT) analysis was performed on the compounds using Gaussian 09 software [36]. In addition, the Swiss ADME tool [37] was used to calculate the molecular properties of the ligands according to the Lipinski rule of five and to evaluate their pharmacokinetic profile.

RESULTS AND DISCUSSION

Target Selection

The Protein Data Bank (PDB) was used to obtain the target crystal structures. Nine different targets (COX-2) were selected for molecular docking experiments, including 1CX2, 3LN0, 3LN1, 3NT1, 4OTJ, 5F1V, 5IKV, 5IKR, and 5KIR. These targets were obtained from both Mus musculus (3LN0, 3LN1, 3NT1, 4OTJ) and Homo sapiens organisms (5F1V, 5IKV, 5IKR, 5KIR). The X-ray ligands for Mus

Table 1. List of Target Proteins, Grid Size (x, y, z), and RMSD Values

PDB ID	X-ray ligand	Resolution (Å)	Species	Grid size (x, y, z) (Å)	RMSD (Å)
1CX2	S58	3.00	Mus musculus	28.612 28.603 9.142	18.8431
3LN0	52B	2.20	Mus musculus	26.339 23.831 15.386	3.0531
3LN1	CEL	2.40	Mus musculus	30.597 -22.559 -15.758	0.8838
3NT1	NPS	1.73	Mus musculus	-40.957 -51.293 -22.318	0.5757
4OTJ	IXP	2.11	Mus musculus	71.166 14.810 138.987	24.0902
5F1A	SAL	2.38	Homo sapiens	38.399 28.789 237.447	16.6014
5IKV	FLF	2.51	Homo sapiens	166.688 186.173 191.675	16.2785
5IKR	ID8	2.34	Homo sapiens	38.042 2.131 61.280	0.9385
5KIR	RCX	2.70	Homo sapiens	23.287 0.439 34.435	14.6685

musculus targets were S58, 52B, CEL, NPS, and IXP, respectively. While the Homo sapiens targets were co-crystallized with the following ligands: SAL, FLF, ID8, and RCX, respectively. Notably, RCX (Rofecoxib) is a selective COX-2 inhibitor. Prior to docking, the target structures were prepared by adding hydrogens and assigning charges using the Gasteiger method in Auto Dock Tools. The ligands were energy minimized and converted to PDBQT format for Auto Dock Vina docking experiments. Table 1 provides the details about the selected targets.

The accuracy of the docking experiments was evaluated by calculating the Root Mean Square Deviation (RMSD) [38] of the best-docked pose of the reference ligand with its crystallographic binding mode. The results are given in Table 1. Two complexes, namely 3NT1@NPX and 5IKR@ID8, were selected for further analysis due to their high resolution (1.73 Å and 2.34 Å, respectively) and good RMSD values (0.5757 Å and 0.9385 Å, respectively).

Visual Analysis

Visual analysis of the selected complexes was performed using Discovery software to confirm the accuracy of the docking results. The predicted ligands (green) and the reference ligands (blue) were perfectly superimposed and well positioned in both the 5IKR and 3NT1 complexes, confirming the low RMSD values (Figs. 2a and 2b). However, the predicted ligand of the 3LN0 complex was poorly positioned with respect to the reference ligand (Fig. 2c), indicating the high RMSD value.

Overall, the 3D structures of all the complexes were

thoroughly analyzed for docking.

Molecular Docking

Docking simulations were executed using Auto Dock Vina through the ADT (Auto dock tools) interface to estimate the binding affinity and binding mode of ligands to selected targets. The Auto Dock Vina affinity values obtained by docking simulations are reported in Table 2.

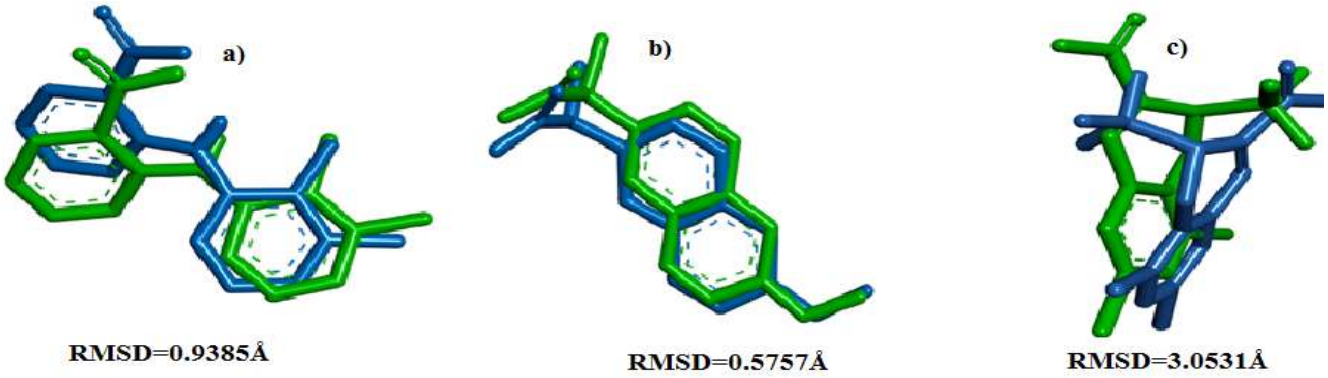

Fig. 2. The best docking pose for: a) ID8 (green) binding to 5IKR, b) NPS (green) binding to 3NT1, c) 52B (green) binding to 3LN0, superimposed with the co-crystallized ligands (blue).

Table 2. Ligands with their Affinity

Targets	5IKR	3TN1	Targets	5IKR	3TN1
LN°	Affinity (kcal mol^{-1})		LN°	Affinity (kcal mol^{-1})	
1	-8.3	-8.5	21	-8.4	-8.4
2	-8.3	-8.4	22	-7.3	-7.7
3	-7.6	-7.4	23	-8.3	-8.2
4	-7.4	-7.5	24	-8.1	-8.3
5	-8.4	-8.8	25	-8.1	-8.5
6	-7.2	-7.5	26	-8.5	-8.1
7	-8.9	-8.5	27	-7.8	-8.0
8	-7.3	-7.2	28	-8.1	-8.2
9	-7.2	-7.2	29	-8.2	-8.1
10	-7.4	-7.7	30	-8.3	-8.3
11	-8.1	-8.6	31	-8.3	-8.7
12	-8.0	-8.2	32	-7.6	-8.4
13	-7.9	-8.4	33	-7.0	-7.0
14	-7.6	-8.0	34	-7.7	-8.2
15	-8.5	-8.1	35	-8.5	-8.5
16	-9.1	-8.4	36	-7.5	-7.9
17	-8.6	-8.8	37	-7.4	-8.6
18	-8.7	*-8.5*	38	-8.0	-8.8
19	-7.9	-8.1	39	-7.2	
20	-7.3	-7.6	40		-7.2

The criterion for selecting the best pose is affinity, the lower the affinity, the more stable the ligand-receptor complex. Based on the results of the molecular docking analysis, all flavonoid compounds (L1-L35) showed a better binding affinity towards the selected receptors (5IKR and 3NT1).

According to results obtained from the molecular docking study, we found significant binding affinity of all flavonoids and drug coxibs (L36, L37, and L38) towards the selected receptors (5IKR and 3NT1).

The flavonoid compounds exhibited superior binding affinity with minimum binding energy values ranging from -7.0 to -9.1 kcal mol^{-1} towards human COX-2 (5IKR), surpassing the co-crystallized ligand, L39 (-7.2 kcal mol^{-1}), and the coxib ligands, L36-L38 (-7.5, -7.4, and -8.0 kcal mol^{-1}, respectively). These results highlight that among all ligands, L16 displayed the highest binding affinity, with a value of -9.1 kcal mol^{-1}, followed by L7 (-8.9 kcal mol^{-1}) and L18 (-8.7 kcal mol^{-1}), respectively.

For the 3NT1 receptor, flavonoid compounds showed binding energies ranging from -7.0 to -8.8 kcal mol^{-1} (Table 2), with the best results obtained with compounds L 5 (-8.8 kcal mol^{-1}) and L 17 (-8.8 kcal mol^{-1}), compared with the X-ray ligand, L 39 (-7.2 kcal mol^{-1}) and the coxib ligands (-7.9, -8.6 and -8.8 kcal mol^{-1}, respectively). According to the results, the stability of the ligand-receptor complexes follows the order of increasing affinity:

receptor@flavonoids < receptor@coxibs < receptor@cocrystallized ligand

The natural flavonoids studied have been shown to form more stable complexes with cyclooxygenase-2 than their selective inhibitors and co-crystallized ligands, indicating that they may be more favorable for inhibition.

The top-performing ligands for the 5IKR complex belong to different classes of flavonoids, namely flavanone (L16), flavone (L7, chrysin dihydroxylation in positions 6 and 8), and flavonol (L18, galangin present in galangal root and hydroxylated in positions 3, 6, and 8). These ligands demonstrated the best interaction affinities among all the tested ligands.

However, for the 3NT1 complex, the best interaction energies are those of the ligands: L5 (-8.8 kcal mol^{-1}), L17 (-8.8 kcal mol^{-1}), and L31 (-8.7 kcal mol^{-1}) hence: of the flavone family (L5: Baicalein, 5,6,7-trihydroxyflavone), Flavonol (L17 and Rhamnetin, L31).

The Baicalein and the Rhamnetin have the same interaction energies with the protein as the Rofecoxib drug (L38).

As can be observed, each class has a different affinity (interaction energy). In comparison to other flavonoid classes and reference ligands, the complexes of hydroxylated flavonoids are more stable. Complex stability is decreased by flavonoid substitution. Reference ligands (L39 and L40) demonstrated the lowest affinity (-7.2 kcal mol^{-1}).

Considering that naproxen (L40) is a potent and non-selective non-steroidal anti-inflammatory drug, frequently prescribed as a prescription drug and used over-the-counter as a Cox-2 inhibitor, it was observed that flavonoids also exhibit various binding patterns, similar to those of synthetic non-steroidal anti-inflammatory drugs. Analysis of the anchored positions of these compounds revealed the presence of different types of binding patterns, reinforcing the similarity between flavonoids and synthetic NSAIDs.

Flavonols such as flavanol and rhamnetin, as well as flavones such as baicalein, demonstrate the presence of a structure containing a catechol part. The docking results between the two selected COXs and the different flavonoids that showed interesting results are shown in Figs. 3 and 4.

Protein-ligand Interactions

In addition, the Discovery interface was used to analyze hydrogen bond interactions, hydrogen bond lengths, and hydrophobic interactions between these compounds and the receptors. The results of this analysis are presented in Table 3.

IKR complex. X-ray ligand: The study of the interaction between target and x-ray ligand is important for comparison with other ligands. The following table represents the different interactions between the active site residues and the reference ligand ID8.

Anne Imbert *et al.* [39] defined strong interactions as those with distances between 2.5 Å and 3.1 Å, medium interactions between 3.1 Å and 3.55 Å, and weak interactions for distances greater than 3.55 Å. Visual analysis of the

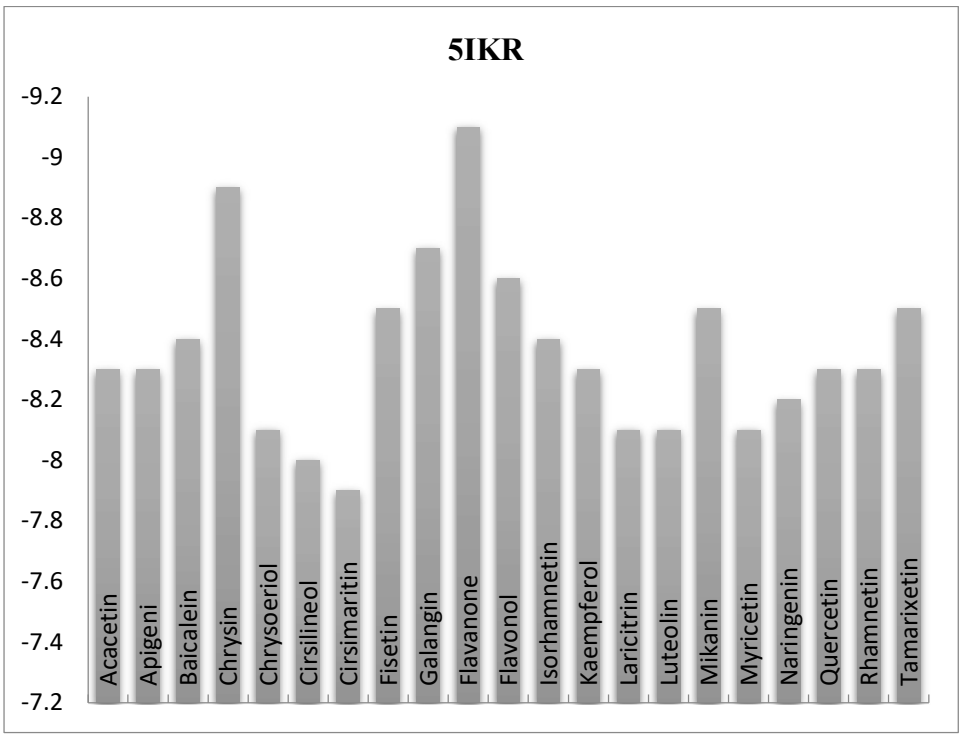

Fig. 3. A vertical bar graph illustrating the adverse binding energies (in Kcal mol^{-1}) for each flavonoid interacting with the active site of human COX (5IKR).

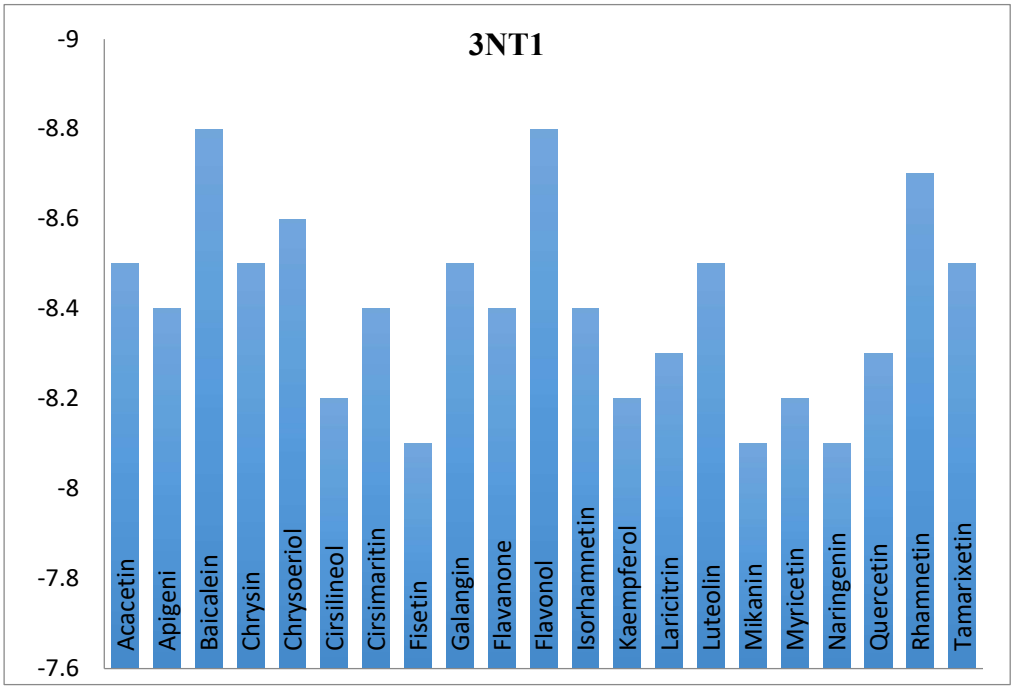

Fig. 4. A vertical bar graph illustrating the adverse binding energies (in Kcal/mol) for each flavonoid interacting with the active site of human COX (3NT1).

Table 3. Intermolecular H-bonding and Hydrophobic Interaction between flavanoids (L5, L7, L16, L17, L18, L31), Coxibs Drugs (L36, L37, L38), co-Crystallized Ligands (L39, L40) and Cox-2 Proteins

N°	Proteins	5IKR			3NT1		
	Ligands	H-bands		Hydrophobe	H-bands		Hydrophobe
		Residues	Distance	Residues	Residues	Distance	Residues
L5	Baicalein	TYR385	2.15	VAL295	TYR385	2.35	VAL444
		ALA199	2.93	HIS388			LEU294
				LEU391	VDW		VAL295
					GLN203		LEU391
							ALA202
L7	Chrysin	SER530	2.08	LEU352	SER530	2.31	TYR355
				GLY526	TYR385	2.77	LEU531
				VAL349	VAL523	3.02	VAL116
							VAL349
							VAL527
							GLY526
							Leu352
L16	Flavanone	SER535	2.45	ALA527	GLN203	3.31	VAL295
		TRY385	2.93	ARG120			LEU391
				VAL349			ALA202
				LEU352			LEU531
							VAL523
							VAL349
							ALA727
							LEU352
							GLY526
L17	Flavonol	SER530	3.63	ALA527	GLN203	3.53	VAL295
				ARG120	TYR385	2.33	LEU391
				VAL349			HIS388
				LEU352			ALA202
				LEU359			
				LEU531			
L18	Galangin	SER530	2.080	LEU531	GLN203	3.53	VAL295
				LEU352	TYR385	2.33	LEU391
				VAL349			HIS388
				VAL523			ALA202
				ALA527			
				GLY526			
L31	Rahmnetin	THR212	2.94	HIS388	ASP125	1.99	APG44
		TRP387	2.75	ALA202	APG44	3.42	LEU152
		KIS388	3.65	HIS207	GLN42	3.60	LYS468
				HIS386	GLU465	1.91	
				VAL447			

Table 3. Continued

L36	Celecoxib	HIS207	3.28	LEU294	HIS207	3.29	VAL444
			2.43	VAL291	GLN203	3.43	LEU408
		ASN222	2.17	LYS211		3.29	LEU294
		THR212	3.36	HIS386			VAL447
		GLIN286	2.32	HIS207			HIS388
		LYS211	3.66				
		ASN382	2.43				
		HIS386	3.21				
		ASN382	2.85				
L37	Rofecoxib	ARG120	3.06	ILE112	GLN203	3.49	VAL295
				TYR115			LEU391
				VAL89			HIS388
L38	Valdicoxib	TYR115	2.08	LYS83	GLN203	3.35	LEU391
		LYS83	3.60	GLU524		3.38	VAL447
		ARG120	1.97	PRO86	HIS207	3.52	VAL295
		PRO86	1.92	ARG120			LEU294
		GLU524	2.10	PRO			HIS388
				VAL89			
L39	ID8	AGR120	2.18	AGR120			
		TRY533	2.02	LYS83			
				VAL89			
				VAL116			
				LEU93			
L40	Naproxen						ALA202
							HIS207
							HIS386
							PHE210

reference ligand (ID8) revealed two conventional hydrogen bonds formed with the active site residues (Fig. 5a).

The first one is a strong H-donor interaction (between the ARG120 residue and the reference ligand oxygen) with a distance of 2.18 Å. The second strong H-acceptor interaction (between residue TYR355 and the OH function of reference ligand) with a distance of 2.02 Å. Hydrophobic bonds are formed with residues LEU93, VAL116, VAL89, LYS83, and PRO86. The 5IKR@ ID8 complex is stabilized by: hydrogen and hydrophobic interactions.

Flavonoids: The docking analysis revealed that the inhibitors used in this study form conventional hydrogen bonds and hydrophobic interactions with the 5IKR binding cavity. Figure 5b illustrates the 3D and 2D interactions of the best-performing flavonoid compounds. The most effective inhibitor, flavanone, is stabilized by two hydrogen bonds with residues TRY385 (2.93 Å) and SER530 (2.45 Å), as well as hydrophobic interactions with amino acids ALA527, ARG120, LEU352, and VAL349. The flavonoids bind with amino acids in the COX-2 active site through hydrogen interactions (SER530) and hydrophobic interactions, mainly with ALA527, GLY526, LEU352, and VAL349.

3NT1 complex. X-ray ligand: Visual analysis of this complex shows that the x-ray ligand formed only hydrophobic interactions with the following four residues: ALA202, HIS207, HIS386, and PHE210 (Fig. 6a).

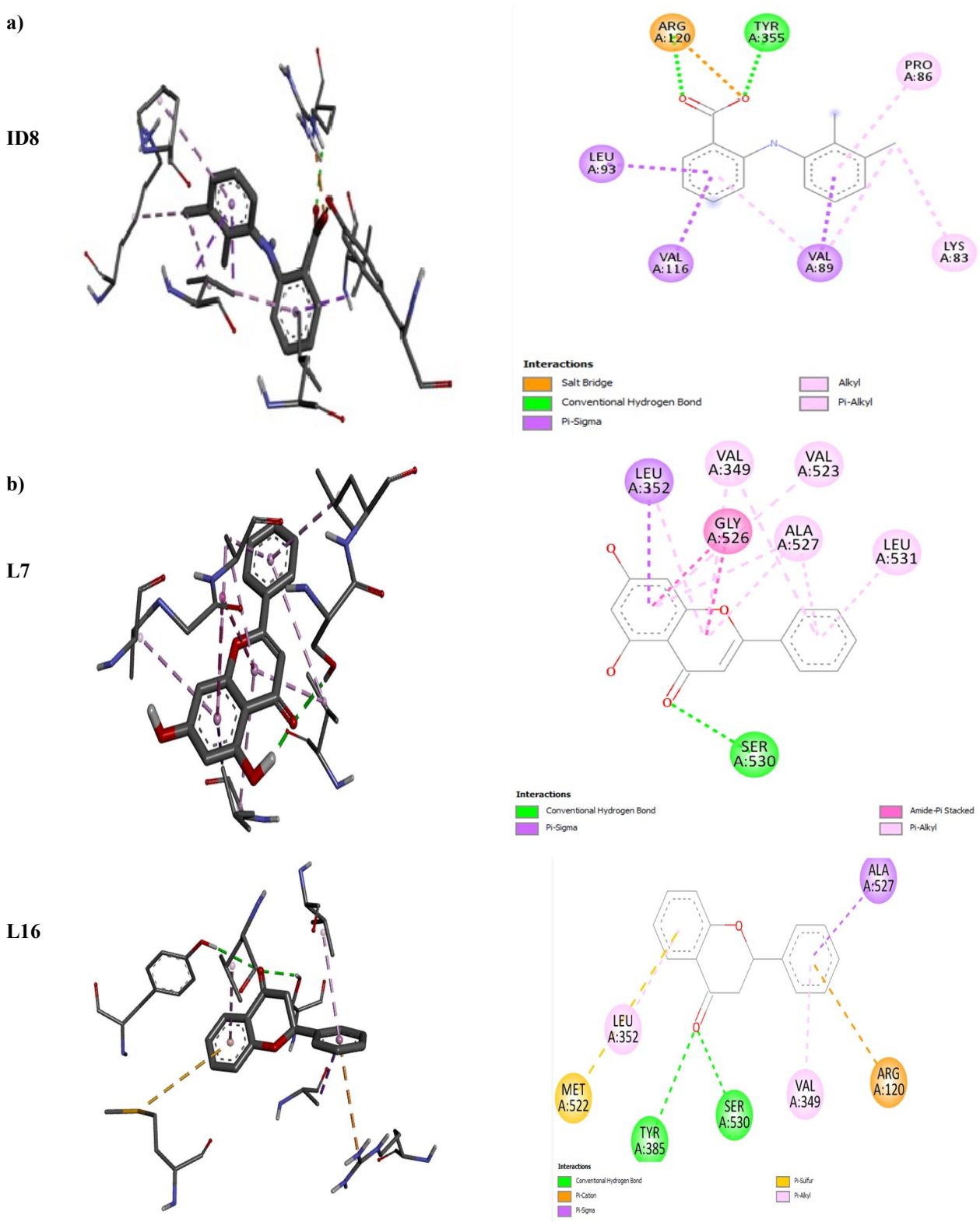

Fig. 5. The 2D and 3D binding interactions ligands of a) ID8, b) L7 and L16 with the target protein (PDB ID: 5IKR), respectively.

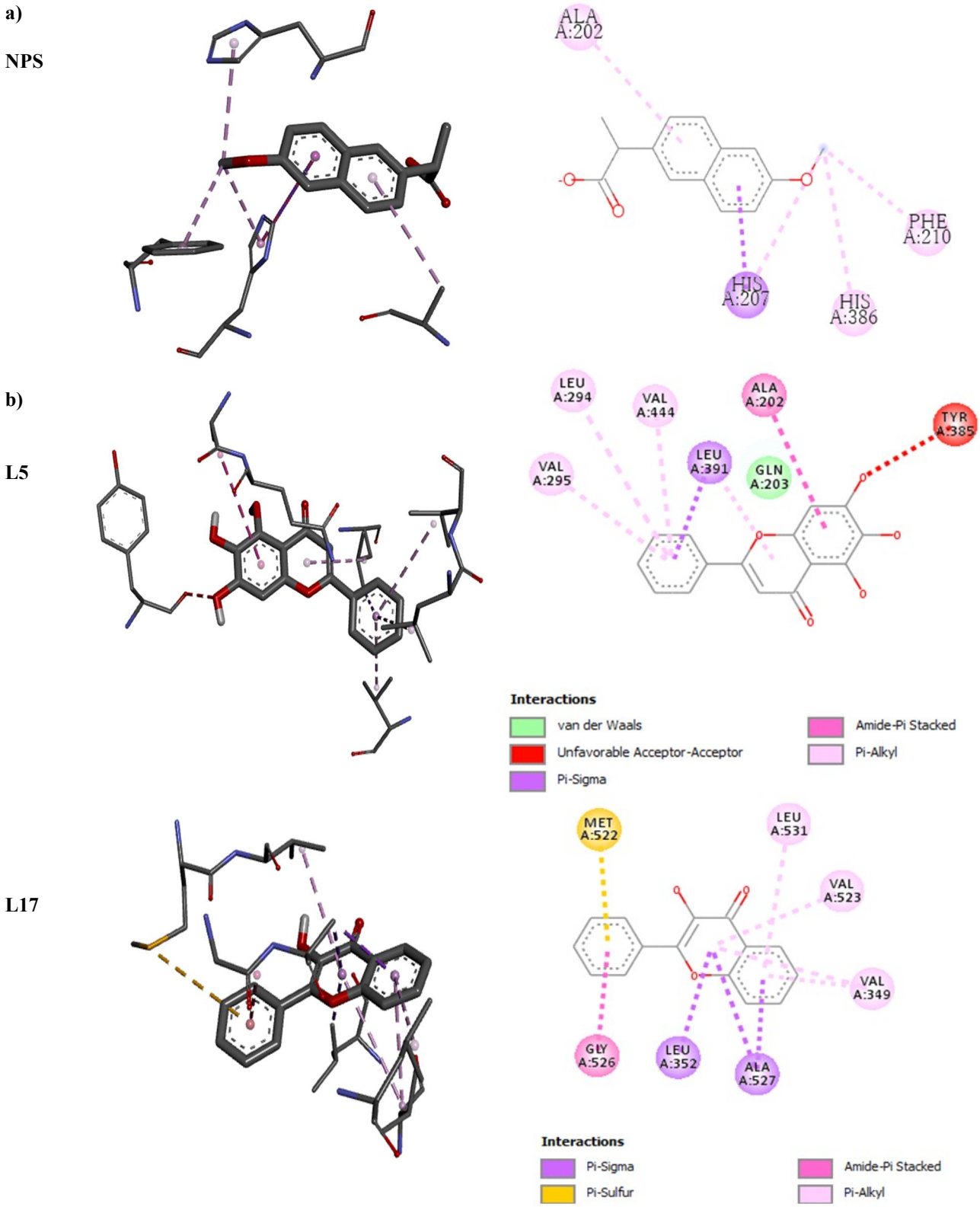

Fig. 6. The 2D and 3D binding interactions ligands of: a) Naproxen, b) Baicalein and Flavonol with the target protein (PDB ID: 3NT1), respectively.

Flavonoids: The active site of 3NT1 accommodates the inhibitors through a combination of hydrogen bonding and hydrophobic interactions. Specifically, the ligand L5 forms two hydrogen bonds with GLN203 and additional hydrophobic interactions, while Ligand L17 is primarily stabilized through hydrophobic interactions. Ligand L31 forms two hydrogen bonds plus the hydrophobic bonds. Notably, all the inhibitors are found in the same region of the active site, forming hydrophobic interactions with several residues and hydrogen bonding with GLN203, the best-performing flavonoid compounds are shown in Fig. 6b.

DFT Analysis

Frontier molecular orbitals (FMO). The electronic properties of molecules, including ionization energy, electronic affinity, hardness, electronegativity, electrophile index, and the HOMO-LUMO energy gap are crucial factors in determining their chemical and physical characteristics.

To optimize the molecules of the best-performing ligands and drugs, we used the DFT method at the B3LYP/6-31G(d,p) level. Table 4 shows the electronic properties of these molecules computed without any symmetrical constraints.

The results indicate that all compounds studied possess a remarkably small energy gap (ΔE), denoting high reactivity. Among the compounds examined, it is observable that flavonoids show the smallest energy gap, registered at 3.621 eV for L31 to 4.796 eV for L16. Conversely, coxibs display the widest energy gaps, which are noted at 4.903 eV, 4.236 eV, and 5.273 eV.

In particular, the energy gap increases in the following order:

Valdecoxib > Rofecoxib > Celecoxib > flavonoids

Finally, L5 retains the highest electrophilicity index (ω), while L16 maintains the lowest.

Flavonoid molecules exhibit higher ionization energy and lower electron affinity.

The smaller energy gaps, lower electron affinities, and higher ionization potentials suggest charge transfer, which impacts the polarizability and biological activities. Regarding the molecules, L16 and L7 demonstrate maximum nucleophilicity, whereas L31 is the most electrophilic. HOMO-LUMO plots are presented in Fig. 7.

Molecular electrostatic potential map (MEP). Using the B3LYP/6-31G(d,p) method, we have calculated the reactive sites for electrophilic and nucleophilic attacks for the best-performing ligands, as shown in Fig. 8. Various colors represent various electrostatic potential values, which allows for a quick visual comparison of potential values in different regions, aiding in the

Table 4. Calculated Values in Electron Volts (eV) of the Electronic Parameters for the Best-performing Ligands

L.N°	Compound	E_{HOMO} (eV)	E_{LUMO} (eV)	IE	EA	ΔE	η	χ	ω
				Best flavonoids					
L5	Baicalein	-5.735	-1.897	5.735	1.897	3.837	1.919	3.816	3.794
L7	Chrysin	-6.001	-1.891	6.001	1.891	4.110	2.055	3.946	3.789
L16	Flavanone	-6.339	-1.544	6.339	1.544	4.796	2.397	3.941	3.240
L17	Flavonol	-5.872	-1.739	5.872	1.739	4.134	2.067	3.806	3.503
L18	Galangin	-5.754	-1.800	5.754	1.800	3.954	1.977	3.777	3.607
L31	Rhamnetin	-5.423	-1.802	5.423	1.802	3.621	1.811	3.613	3.604
				Coxibs drugs					
L36	Celecoxib	-6.505	-1.602	6.505	1.602	4.903	2.451	4.054	3.351
L37	Rofecoxib	-6.587	-2.352	6.587	2.352	4.236	2.118	4.469	4.716
L38	Valdecoxib	-6.624	-1.352	6.624	1.352	5.273	2.636	3.988	3.017

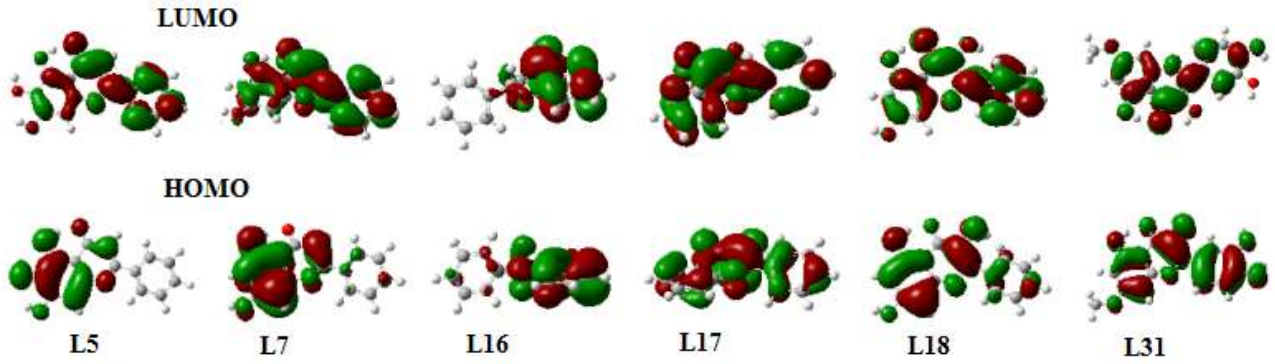

Fig. 7. HOMO-LUMO plots of flavonoid compounds.

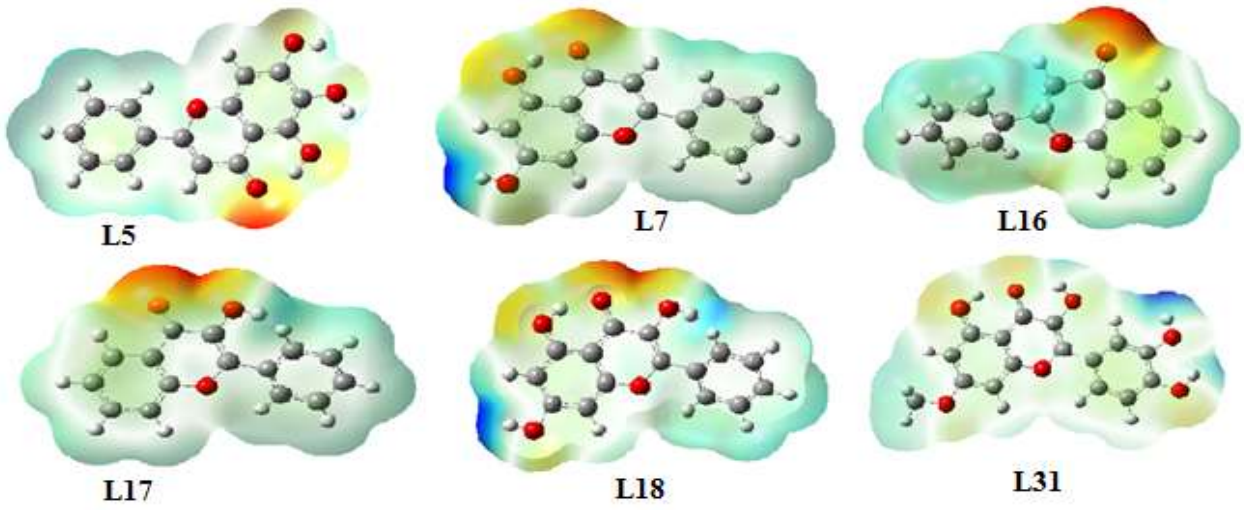

Fig. 8. Flavonoid compounds MEP plots.

interpretation of electrostatic potential data. The most intense repulsion (negative phase) is depicted in red, while the most pronounced attraction (positive phase) is denoted by blue. The MEP map of the titrated compound reveals that the oxygen atoms align with the regions of the strongest repulsion, signifying the nucleophilic zones of the molecules. These regions can form stabilizing connections with neighboring molecules, including hydrogen bonds and other electrostatic bonds.

Drug-likeness of the Ligands

Drug-likeness filters are crucial in early preclinical development to prevent costly failures later on. The drug-likeness of selected flavonoid compounds was assessed using Lipinski's Rule of Five, and all met the criteria. Lipinski's Rule of Five is a guideline based on the observation that successful drugs generally have specific molecular characteristics. These include a molecular weight of around 500 or less, logP values not exceeding 5, no more than 5 hydrogen donor sites, and no more than 10 hydrogen bond acceptor sites. Other factors like polar surface area and the number of rotary bonds are also linked to drug bioavailability.

ADME Predictions

Furthermore, understanding gastrointestinal (GI) and blood-brain barrier (BBB) permeation is crucial for assessing the absorption and distribution of drug molecules [13,40].

Table 5. Physicochemical Properties of Flavonoids with Better Affinity, Computed by Swiss ADME

Ligand N°	Flavonoid compound	MW (g mol^{-1})	logP (ilogP)	TPSA Å²	HD	HA	RB	Lipinski's violations
Rule		< 500	≤ 5	< 140	< 5	< 10	< 5	≤ 1
L5	Baicalein	270.24	1.89	90.90	3	5	1	0
L7	Chrysin	254.24	2.27	70.67	2	4	1	0
L16	Flavanone	224.25	2.41	26.30	0	2	1	0
L17	Flavonol	238.24	2.44	50.44	1	3	1	0
L18	Galangin	270.24	2.08	90.90	3	5	1	0
L31	Rhamnetin	316.26	2.23	120.36	4	7	2	0

Abbreviations: MW: molecular weight (g mol^{-1}); HD, number of hydrogen donors; HA, number of hydrogen acceptors; RB, number of rotatable bonds; TPSA, total polar surface area (Å²).

Table 6. Pharmacokinetics Parameters and Bioavailability of Flavonoids

Parameters	Ligands/Flavonoids					
	L5	L7	L16	L17	L18	L31
	Baicalein	Chrysin	Flavanone	Flavonol	Galangin	Rhamnetin
GI absorption	High	High	High	High	High	High
BBB permeant	No	Yes	Yes	Yes	No	No
P-gp substrate	No	No	No	No	No	No
CYP1A2	Yes	Yes	Yes	Yes	Yes	Yes
CYP2C19	No	No	No	Yes	No	No
CYP2C9	No	No	No	No	No	No
CYP2D6	Yes	Yes	No	Yes	Yes	Yes
CYP3A4	Yes	Yes	No	Yes	Yes	Yes
logK_p (cm/s) (skin permeation)	-5.70	-5.35	-5.44	-5.34	-6.35	-6.90
Bioavailability Score	0.55	0.55	0.55	0.55	0.55	0.55

The *in silico* predictions for absorption, distribution, metabolism, and excretion (ADME) of the studied structures are summarized in Table 6.

Swiss ADME predictions show high gastrointestinal (GI) absorption for all compounds. Specifically, compounds L7, L16, and L17 demonstrated blood-brain barrier (BBB) permeation, whereas compounds L5, L18, and L31 did not. Additionally, not all compounds serve as substrates for Permeability glycoprotein (P-gp), and this information is essential for estimating active efflux through biological membranes, such as from the gastrointestinal wall to the lumen or from the brain.

The metabolism of drug molecules is regulated by a variety of cytochromes (CYP's), with CYP1A2, CYP2C19, CYP2C9, CYP2D6, and CYP3A4 playing vital roles [13, 41]. In the in-silico SwissADME prediction, compound L17 inhibited all cytochromes except CYP2C9. Compounds L5, L7, L18, and L31 inhibited CYP1A2, CYP2D6, and CYP3A4, while compound L16 inhibited only CYP1A2.

The skin permeability value (Kp) in cm s^{-1} serves as an

indicator of the absorption of molecules through the skin. *In silico*, the skin permeability, represented by logKp values, ranged from -5.34 to -6.90 cm s^{-1} for all compounds, indicating a low degree of skin permeability. The more negative the $logK_p$, the less the molecule permeates the skin. All flavonoids were found to be impermeable through the skin. This indicates a favorable pharmacokinetic profile for these compounds.

CONCLUSION

Several flavonoids from the chemical classes flavonol, flavone, and flavanone were tested for inhibitory activity against COX-2 target proteins in this study. Based on docking scores and interaction analysis, most of these compounds were found to be effective in inhibiting the COX active site. Notably, all flavonoids displayed significantly higher binding affinities compared to coxib compounds, which are commonly used as anti-inflammatory drugs.

Among the flavonoids, flavanone exhibited the highest binding affinity (-9.1 kcal mol^{-1}) towards the amino acids in the human COX active site through hydrogen interactions and hydrophobic interactions.

The distribution of charges in the Highest Occupied Molecular Orbital (HOMO) and Lowest Unoccupied Molecular Orbital (LUMO) energy levels implies the existence of intramolecular charge transfer in certain molecules. The reduced HOMO-LUMO energy gap in the titled compounds implies a higher reactivity compared to coxib compounds.

The investigation of Molecular Electrostatic Potential (MEP) maps for the flavanone molecule reveals a negative potential surrounding the oxygen atom within the carbonyl group. Consequently, this specific site is identified as the favored location for electrophilic attacks.

Flavonoid compounds underwent assessment for the rule of five and ADME properties. Pharmacokinetic screening of the chosen compounds indicated adherence to Lipinski's rule of five without any violations, suggesting their potential as candidate drug molecules.

The findings derived from molecular docking, drug-likeness evaluation, ADME analysis, and DFT calculations suggest that studies on flavonoids indicate their potential as drugs, showcasing noteworthy biological activities.

ACKNOWLEDGMENTS

This study was not supported financially by any grants.

REFERENCES

[1] Howe, L. R., Inflammation and Breast Cancer. Cyclooxygenase/Prostaglandin Signaling and Breast Cancer. *Breast Cancer Res.* **2007**, *9* (4), 210, https://doi.org/10.1186/bcr1678.

[2] Xiao, X.; Shi, D.; Liu, L.; Wang, J.; Xie, X.; Kang, T.; Deng, W., Quercetin Suppresses Cyclooxygenase-2 Expression and Angiogenesis through Inactivation of P300 Signaling. *PLoS ONE*. **2011**, *6* (8), e22934, https://doi.org/10.1371/journal.pone.0022934.

[3] Abdellatif, K. R. A.; Abdelall, E. K. A.; Fadaly, W. A. A.; Kamel, G. M., Synthesis, Cyclooxygenase Inhibition, Anti-Inflammatory Evaluation and Ulcerogenic Liability of New 1,3,5-Triarylpyrazoline and 1,5-Diarylpyrazole Derivatives as Selective COX-2 Inhibitors. *Bioorg. Med. Chem. Lett.* **2016**, *26* (2), 406-412, https://doi.org/10.1016/j.bmcl.2015.11.105.

[4] Ahmadi, M.; Bekeschus, S.; Weltmann, K.-D.; von Woedtke, T.; Wende, K., Non-Steroidal Anti-Inflammatory Drugs: Recent Advances in the Use of Synthetic COX-2 Inhibitors. *RSC Med. Chem.* **2022**, *13* (5), 471-496, https://doi.org/10.1039/D1MD00280E.

[5] Arora, M.; Choudhary, S.; Singh, P. K.; Sapra, B.; Silakari, O., Structural Investigation on the Selective COX-2 Inhibitors Mediated Cardiotoxicity: A Review. *Life Sci.* **2020**, *251*, 117631, https://doi.org/10.1016/j.lfs.2020.117631.

[6] Chen, W.; Zhong, Y.; Feng, N.; Guo, Z.; Wang, S.; Xing, D., New Horizons in the Roles and Associations of COX-2 and Novel Natural Inhibitors in Cardiovascular Diseases. *Mol. Med.* **2021**, *27* (1), 123, https://doi.org/10.1186/s10020-021-00358-4.

[7] Kaur, A.; Pathak, D. P.; Sharma, V.; Wakode, S., Synthesis, Biological Evaluation and Docking Study of a New Series of Di-Substituted Benzoxazole Derivatives as Selective COX-2 Inhibitors and Anti-Inflammatory Agents. *Bioorg. Med. Chem.* **2018**, *26* (4), 891-902, https://doi.org/10.1016/j.bmc.2018.01.007.

[8] Md Idris, M. H.; Mohd Amin, S. N.; Mohd Amin, S. N.; Nyokat, N.; Khong, H. Y.; Selvaraj, M.; Zakaria, Z. A.; Shaameri, Z.; Hamzah, A. S.; Teh, L. K.; *et al*., Flavonoids as Dual Inhibitors of Cyclooxygenase-2 (COX-2) and 5-Lipoxygenase (5-LOX): Molecular Docking and in Vitro Studies. *Beni-Suef Univ. J. Basic Appl. Sci.* **2022**, *11* (1), 117, https://doi.org/10.1186/s43088-022-00296-y.

[9] Baek, S. -H.; Hwang, S.; Park, T.; Kwon, Y. -J.; Cho, M.; Park, D., Evaluation of Selective COX-2 Inhibition and In Silico Study of Kuwanon Derivatives Isolated from Morus Alba. *Int. J. Mol. Sci.* **2021**, *22* (7), 3659, https://doi.org/10.3390/ijms22073659.

[10] Rayar, A. M.; Lagarde, N.; Martin, F.; Blanchard, F.; Liagre, B.; Ferroud, C.; Zagury, J. -F.; Montes, M.; Sylla-Iyarreta Veitía, M., New Selective Cyclooxygenase-2 Inhibitors from Cyclocoumarol: Synthesis, Characterization, Biological Evaluation and Molecular Modeling. *Eur. J. Med. Chem.* **2018**, *146*, 577-587, https://doi.org/10.1016/j.ejmech.2018.01.054.

[11] Mandour, Y.; Handoussa, H.; Swilam, N.; Hanafi, R.; Mahran, L., Structural Docking Studies of COX-II Inhibitory Activity for Metabolites Derived from *Corchorus Olitorius* and *Vitis Vinifera*. *Int. J. Food Prop.* **2016**, *19* (10), 2377-2384, https://doi.org/10.1080/10942912.2015.1114492.

[12] Cushnie, T. P. T.; Lamb, A. J., Antimicrobial Activity of Flavonoids. *Int. J. Antimicrob. Agents*. **2005**, *26* (5), 343-356, https://doi.org/10.1016/j.ijantimicag.2005.09.002.

[13] Farhadi, F.; Khameneh, B.; Iranshahi, M.; Iranshahy, M., Antibacterial Activity of Flavonoids and Their Structure-Activity Relationship: An Update Review. *Phytother. Res.* **2019**, *33* (1), 13-40, https://doi.org/10.1002/ptr.6208.

[14] Zakaryan, H.; Arabyan, E.; Oo, A.; Zandi, K., Flavonoids: Promising Natural Compounds against Viral Infections. *Arch. Virol.* **2017**, *162* (9), 2539-2551, https://doi.org/10.1007/s00705-017-3417-y.

[15] Bai, H. -W.; Zhu, B. T., Strong Activation of Cyclooxygenase I and II Catalytic Activity by Dietary Bioflavonoids. *J. Lipid Res.* **2008**, *49* (12), 2557-2570, https://doi.org/10.1194/jlr.M800358-JLR200.

[16] Orlando, B. J.; Malkowski, M. G., Crystal Structure of Rofecoxib Bound to Human Cyclooxygenase-2. *Acta Crystallogr. Sect. F Struct. Biol. Commun.* **2016**, *72* (10), 772-776, https://doi.org/10.1107/S2053230X16014230.

[17] Rudrapal, M.; Eltayeb, W. A.; Rakshit, G.; El-Arabey, A. A.; Khan, J.; Aldosari, S. M.; Alshehri, B.; Abdalla, M., Dual Synergistic Inhibition of COX and LOX by Potential Chemicals from Indian Daily Spices Investigated through Detailed Computational Studies. *Sci. Rep.* **2023**, *13* (1), 8656. https://doi.org/10.1038/s41598-023-35161-0.

[18] Jain, A. S.; Sushma, P.; Dharmashekar, C.; Beelagi, M. S.; Prasad, S. K.; Shivamallu, C.; Prasad, A.; Syed, A.; Marraiki, N.; Prasad, K. S., *In Silico* Evaluation of Flavonoids as Effective Antiviral Agents on the Spike Glycoprotein of SARS-CoV-2. *Saudi J. Biol. Sci.* **2021**, *28* (1), 1040-1051, https://doi.org/10.1016/j.sjbs.2020.11.049.

[19] Sadati, S.; Gheibi, N.; Ranjbar, S.; Hashemzadeh, M., Docking Study of Flavonoid Derivatives as Potent Inhibitors of Influenza H1N1 Virus Neuraminidase. *Biomed. Rep.* **2018**, https://doi.org/10.3892/br.2018.1173.

[20] Chahal, S.; Rani, P.; Kiran; Sindhu, J.; Joshi, G.; Ganesan, A.; Kalyaanamoorthy, S.; Mayank; Kumar, P.; Singh, R.; et al., Design and Development of COX-II Inhibitors: Current Scenario and Future Perspective. *ACS Omega*. **2023**, *8* (20), 17446-17498. https://doi.org/10.1021/acsomega.3c00692.

[21] Consalvi, S.; Alfonso, S.; Di Capua, A.; Poce, G.; Pirolli, A.; Sabatino, M.; Ragno, R.; Anzini, M.; Sartini, S.; La Motta, C.; et al., Synthesis, Biological Evaluation and Docking Analysis of a New Series of Methylsulfonyl and Sulfamoyl Acetamides and Ethyl Acetates as Potent COX-2 Inhibitors. *Bioorg. Med. Chem.* **2015**, *23* (4), 810-820, https://doi.org/10.1016/j.bmc.2014.12.041.

[22] Dash, R.; Uddin, M. M.; Hosen, S. M. Z.; Rahim, Z. B.; Dinar, A.; *et al*., Molecular Docking Analysis of Known Flavonoids as Duel COX-2 Inhibitors in the Context of Cancer. *Bioinformation*. **2015**, *11* (12), 543-549, https://doi.org/10.6026/97320630011543.

[23] Surendar, P.; Pooventhiran, T.; Rajam, S.;

Bhattacharyya, U.; Bakht, Md. A.; Thomas, R., Quasi Liquid Schiff Bases from Trans-2-Hexenal and Cytosine and l-Leucine with Potential Antieczematic and Antiarthritic Activities: Synthesis, Structure and Quantum Mechanical Studies. *J. Mol. Liq.* **2021**, *334*, 116448. https://doi.org/10.1016/j.molliq.2021.116448.

[24] Thadathil, D. A.; Varghese, S.; Akshaya, K. B.; Thomas, R.; Varghese, A., An Insight into Photophysical Investigation of (E)-2-Fluoro-N'-(1-(4-Nitrophenyl) Ethylidene)Benzohydrazide through Solvatochromism Approaches and Computational Studies. *J. Fluoresc.* **2019**, *29* (4), 1013-1027. https://doi.org/10.1007/s10895-019-02415-y.

[25] P. R., K. R.; Mary, Y. S.; Fernandez, A.; S, A. P.; Mary, Y. S.; Thomas, R., Single Crystal XRD, DFT Investigations and Molecular Docking Study of 2-((1,5-Dimethyl-3-Oxo-2-Phenyl-2,3-Dihydro-1H-Pyrazol-4-Yl) Amino)Naphthalene-1,4-Dione as a Potential Anti- Cancer Lead Molecule. *Comput. Biol. Chem.* **2019**, *78*, 153-164. https://doi.org/10.1016/j.compbiolchem.2018.11.022.

[26] John, A. M.; Jose, J.; Thomas, R.; Thomas, K. J.; Balakrishnan, S. P., Spectroscopic and TDDFT Investigation of Highly Selective Fluoride Sensors by Substituted Acyl Hydrazones. *Spectrochim. Acta. A. Mol. Biomol. Spectrosc.* **2020**, *236*, 118329. https://doi.org/10.1016/j.saa.2020.118329.

[27] 27- Sheena Mary, Y.; Ertan-Bolelli, T.; Thomas, R.; Krishnan, A. R.; Bolelli, K.; Kasap, E. N.; Onkol, T.; Yildiz, I., Quantum Mechanical Studies of Three Aromatic Halogen-Substituted Bioactive Sulfonamidobenzoxazole Compounds with Potential Light Harvesting Properties. *Polycycl. Aromat. Compd.* **2021**, *41* (7), 1563-1579. https://doi.org/10.1080/10406638.2019.1689405.

[28] Surendar, P.; Pooventhiran, T.; Al-Zaqri, N.; Rajam, S.; Jagadeeswara Rao, D.; Thomas, R., Synthesis of Three Quasi Liquid Schiff Bases between Hexanal and Adenine, Cytosine, and l-Leucine, Structural Interpretation, Quantum Mechanical Studies and Biological Activity Prediction. *J. Mol. Liq.* **2021**, *341*, 117305. https://doi.org/10.1016/j.molliq.2021.117305.

[29] Alsalme, A.; Pooventhiran, T.; Al-Zaqri, N.; Rao, D. J.; Rao, S. S.; Thomas, R., Modelling the Structural and Reactivity Landscapes of Tucatinib with Special Reference to Its Wavefunction-Dependent Properties and Screening for Potential Antiviral Activity. *J. Mol. Model.* **2020**, *26* (12), 341. https://doi.org/10.1007/s00894-020-04603-1.

[30] Aazam, E. S.; Thomas, R., Solution Stage Fluorescence and Anticancer Properties of Azomethine Compounds from Sulpha Drugs: Synthesis, Experimental and Theoretical Insights. *J. Mol. Struct.* **2024**, *1295*, 136669. https://doi.org/10.1016/j.molstruc.2023.136669.

[31] Afroz Bakht, Md.; Alharthi, A. I.; Thangaiyan, P.; Ahmad, A.; Ali, I.; Thomas, R., Interaction of Serotonin and Histamine with Water and Ethanol: Evidence from Theoretical Investigations. *Comput. Theor. Chem.* **2023**, *1228*, 114299. https://doi.org/10.1016/j.comptc.2023.114299.

[32] Al-Hakim Badawi, M. A.; Al-Zaben, M. I.; Thomas, R., DFT Studies on Mechanism of Organocatalytic Metal-Free Click 32CA Reaction for Synthesis of NH-1,2,3-triazoles. *Catal Lett.* **2023**. https://doi.org/10.1007/s10562-023-04374-3.

[33] Trott, O.; Olson, A. J., AutoDock Vina: Improving the Speed and Accuracy of Docking with a New Scoring Function, Efficient Optimization, and Multithreading. *J. Comput. Chem.* **2010**, *31* (2), 455-461. https://doi.org/10.1002/jcc.21334.

[34] Discovery Studio BIOVA, Discov. Stud. Client V17, San Diego, Dassault Syst. (2017). http://accelrys.com/products/collaborative-science/biovia-discoverystudio/.

[35] Di Muzio, E.; Toti, D.; Polticelli, F. DockingApp: A user friendly interface for facilitated docking simulations with Auto Dock Vina. *J. Comput. Aided Mol. Des.* **2017**, *31*, 213-218.

[36] M. J. Frisch, G. W. Trucks, H. B. Schlegel, G. E. Scuseria, M. A. Robb, J. R. Cheeseman, G. Scalmani, V. Barone, B. Mennucci, G. A. Petersson, H. Nakatsuji, M. Caricato, X. Li, H. P. Hratchian, A. F. Izmaylov, J. Bloino, G. Zheng, J. L. Sonnenberg, M. Hada, M. Ehara, K. Toyota, R. Fukuda, J. Hasegawa, M. Ishida, T. Nakajima, Y. Honda, O. Kitao, H. Nakai, T. Vreven, J. A. Montgomery Jr., J. E. Peralta, F. Ogliaro, M. Bearpark, J. J. Heyd, E. Brothers, K. N. Kudin, V. N.

Staroverov, R. Kobayashi, J. Normand, K. Raghavachari, A. Rendell, J. C. Burant, S. S. Iyengar, J. Tomasi, M. Cossi, N. Rega, J. M. Millam, M. Klene, J. E. Knox, J. B. Cross, V. Bakken, C. Adamo, J. Jaramillo, R. Gomperts, R. E. Stratmann, O. Yazyev, A. J. Austin, R. Cammi, C. Pomelli, J. W. Ochterski, R. L. Martin, K. Morokuma, V. G. Zakrzewski, G. A. Voth, P. Salvador, J. J. Dannenberg, S. Dapprich, A. D. Daniels, O. Farkas, J. B. Foresman, J. V Ortiz, J. Cioslowski, D. J. Fox, Gaussian09 Revision D.01, 2013.

[37] Daina, A.; Michielin, O.; Zoete, V., SwissADME: A free web tool to evaluate pharmacokinetics, drug-likeness and medicinal chemistry friendliness of small molecules. *Sci. Rep.* **2017**, *7*, 42717. http://www.swissadme.ch/index.php/.

[38] Bursulaya, B. D.; Totrov, M.; Abagyan, R.; Brooks III, C. L., Comparative Study of Several Algorithms for Flexible Ligand Docking. *J. Comput. Aided Mol. Des.* **2003**, *17* (11), 755-763, https://doi.org/10.1023/B:JCAM.0000017496.76572.6f.

[39] Imberty, A.; Hardman, K. D.; Carver, J. P.; Perez, S., Molecular Modelling of Protein-Carbohydrate Interactions. Docking of Monosaccharides in the Binding Site of Concanavalin A. *Glycobiology*. **1991**, *1* (6), 631-642, https://doi.org/10.1093/glycob/1.6.631.

[40] Eswaramoorthy, R.; Hailekiros, H.; Kedir, F.; Endale, M., *In Silico* Molecular Docking, DFT Analysis and ADMET Studies of Carbazole Alkaloid and Coumarins from Roots of Clausena Anisata: A Potent Inhibitor for Quorum Sensing. *Adv. Appl. Bioinforma. Chem.* **2021**, *Volume 14*, 13-24, https://doi.org/10.2147/AABC.S290912.

[41] Das, P.; Majumder, R.; Mandal, M.; Basak, P., *In-Silico* Approach for Identification of Effective and Stable Inhibitors for COVID-19 Main Protease from Flavonoid Based Phytochemical Constituents of *Calendula Officinalis*. *J. Biomol. Struct. Dyn.* **2021**, *39* (16), 6265-6280, https://doi.org/10.1080/07391102.2020.1796799.